Journal of Power Sources 243 (2013) 48–53

Contents lists available at SciVerse ScienceDirect

Journal of Power Sources

journal homepage: www.elsevier.com/locate/jpowsour

Smaller Pt particles supported on mesoporous bowl-like carbon for highly efficient and stable methanol oxidation and oxygen reduction reaction

Zaoxue Yan [a], Mingmei Zhang [a], Jimin Xie [a,*], Hongen Wang [b], Wei Wei [a]

[a] School of Chemistry and Chemical Engineering, Jiangsu University, Zhenjiang 212013, PR China
[b] State Key Laboratory of Advanced Technology for Materials Synthesis and Processing, Wuhan University of Technology, Wuhan 430070, PR China

HIGHLIGHTS

- Mesoporous bowl-like carbons (BLCs) are synthesized.
- The BLCs have surface area of 1108.3 $m^2\ g^{-1}$ and pore volume of 2.7 $cm^3\ g^{-1}$.
- The BLCs favor dispersion and stable loading of smaller Pt particles.
- The Pt/BLC shows high activity and stability for methanol oxidation and ORR.

ARTICLE INFO

Article history:
Received 20 April 2013
Received in revised form
2 June 2013
Accepted 3 June 2013
Available online 12 June 2013

Keywords:
Mesoporous bowl-like carbon
Methanol oxidation
Oxygen reduction reaction
Platinum electrocatalyst
Fuel cell
Electrocatalytic stability

ABSTRACT

Bowl-like carbons (BLCs) with mesoporous structure are prepared using glucose as carbon source and solid core mesoporous shell silica spheres (SCMSSs) as templates. Pt particles are then loaded on the BLCs as electrocatalyst and used for both methanol oxidation and oxygen reduction reaction (ORR) in acidic media. Physical measurements display that the BLCs are formed due to flowing of melted glucose along the mesoporous shell of the SCMSSs. Moreover, the BLCs with high surface area (1108.3 $m^2\ g^{-1}$), large pore volume (2.7 $cm^3\ g^{-1}$) and mesoporous structure (9.4 nm in diameter) are beneficial for uniform dispersion and stable loading of smaller noble metal particles, and efficiently improve the mass transfer in catalytic reactions, compared to carbon powders. Cyclic voltammogram measurements show that the mass current densities on Pt/BLC electrocatalyst are 2.6 times (1846 mA mg_{Pt}^{-1}) for methanol oxidation and 1.6 times (180.6 mA mg_{Pt}^{-1}) for ORR as high as that of commercial Pt/C (TKK). Furthermore, the mesopores give Pt/BLC more electrocatalytic stability due to stronger physical interaction force.

1. Introduction

The industrialization of low temperature fuel cells like direct alcohol fuel cells is hindered by the electrocatalyst [1–3]. Noble metals such as Pd and Pt have been remaining the main active ingredients of electrocatalyst due to the relative high catalytic activity and stability [4–11]. However, the high cost, low use ratio and poor mass transfer restrict the noble metal based electrocatalyst in both anodic and cathodic electrodes of fuel cells. Therefore, the particle dispersion and size distribution of noble metals, and spatial configuration of the electrocatalyst should be seriously controlled in order to obtain improved use ratio of noble metals, as well as mass transfer of the electrocatalyst, and consequently lower the cost [12–15].

As known, electrochemical reaction takes place at the interface between reactants, catalyst and electrolyte. So, not all the geometric surface of the catalyst work in the electrocatalysis. Only the active ingredients that are exposed to reactants are electrochemically active, while the noble metals inaccessible to reactants are invalid, which obviously decreases the use ratio of noble metals and increases the cost [16].

To address the problem, the morphology and nanostructure of supporting materials are considered to be important factors [17–22]. Carbon materials such as nanotubes [23,24], nanospheres [25], honeycomb-like carbon [26], nanofibers [27], graphene [28,29] and hollow spheres [30,31] have been paid much attention as ideal electrocatalyst supports due to their high surface area, low density, high chemical stability, excellent electric conductivity and

* Corresponding author. Tel.: +86 11 88791708; fax: +86 11 88791800.
E-mail addresses: Xiejm391@sohu.com, earlylearn@163.com (J. Xie).

0378-7753/$ – see front matter © 2013 Elsevier B.V. All rights reserved.
http://dx.doi.org/10.1016/j.jpowsour.2013.06.008

controllable structure. Among them, carbons with mesoporous structure have been extensively investigated due to their excellent mass transfer properties and structural effect on the loaded active ingredients [32–36]. Joo et al. found that the mesoporous carbon with high surface area served the best in terms of high Pt dispersion and electrocatalytic activity [32]. Liu et al. reported that Pt nanoparticles supporting on ordered mesoporous carbon has improved dispersion than that of Pt supporting on Vulcan XC-72 carbon [37]. Song et al. pointed out that electrocatalyst support with mesopores greatly favors the electrochemical activity of alcohol oxidation due to improved mass transfer [38].

Here, we report the synthesis of mesoporous bowl-like carbons (BLCs), which are found favorable for the formation and stable attachment of smaller Pt nanoparticles, as well as improved mass transfer property. Consequently, Pt supporting on BLCs exhibits much higher electrocatalytic activity and stability than that of Pt supporting on carbon powders.

2. Experimental

2.1. Preparation of BLCs

Solid core mesoporous shell silica spheres (SCMSSs) were used as templates for the preparation of BLCs. In the present study, the SCMSSs were prepared according to the procedures reported in the literature [39]. Typically, SCMSSs (1.0 g), glucose (0.5 g) and deionized water (100 ml) were mixed in a flask with vigorous stirring in 70 °C until the mixture turned into a dry solid cake. Subsequently, the cake was heated in nitrogen atmosphere with a heating rate of 2 °C min^{-1} from 100 °C to 200 °C to make glucose melted and flow down along the mesopores of the templates. The sample was then heated to 900 °C with a heating rate of 10 °C min^{-1} and held at that temperature for 1 h to carbonize the glucose. The SCMSS templates were finally removed by etching in HF solution to obtain the BLCs.

2.2. Preparation of Pt/BLC electrocatalyst

Pt supported on the BLCs (denoted as Pt/BLC) or Vulcan XC-72 carbon (denoted as Pt/C (Syns)) was prepared. Typically, BLCs or Vulcan XC-72 carbon (50 mg) were added to mixture of H_2PtCl_4 (containing 50 mg Pt) and 20 ml glycol and dispersed to uniform ink in ultrasonic bath for 30 min, the pH of the mixture was adjusted to 10 by 5 wt% NaOH/glycol solution and put into a microwave oven (700 W) for heating at a 12 s on and 12 s off procedure for 9 times. Afterward, the mixture was washed with deionized water and dried in vacuum at 60 °C for 4 h. The Pt content in the resulting product was targeted at 50 wt%. The actual Pt content was determined by inductively coupled plasma-atomic emission spectrometry (ICP, VISTA-MPX, Austria).

2.3. Electrochemical characterization

4 mg of Pt/BLC, Pt/C (Syns) or commercial Pt/C (TKK, Japan) was dispersed in 1.95 ml ethanol and 0.05 ml 5 wt% Nafion suspension (DuPont, USA) under ultrasonic agitation to form the electrocatalyst ink.

For methanol oxidation, the electrocatalyst ink (5 μl) was deposited on a glassy carbon rod and dried at room temperature. The total Pt loadings were controlled at 0.02 mg cm^{-2}. The electrochemical measurements were performed in a three-electrode cell on a potentiostat at 30 °C with the mixed solution of 0.5 mol L^{-1} H_2SO_4 and 1.0 mol L^{-1} methanol solution as electrolyte. A platinum foil (1.0 cm^2) and saturated calomel electrode (SCE) were used as counter and reference electrodes, respectively.

For ORR, the electrocatalyst ink (5 μl) was deposited on a rotating disk electrode and dried at room temperature. The total Pt loadings were also controlled at 0.02 mg cm^{-2}. The electrochemical measurements were performed in an oxygen-saturated 0.1 mol L^{-1} $HClO_4$ solution scanned between 0 to 1.1 V (vs. RHE) at a scan rate of 5 mV s^{-1} at 25 °C. A platinum foil (1.0 cm^2) and a reversible hydrogen electrode (RHE) were used as counter and reference electrodes, respectively.

2.4. Physical characterization

The morphologies and sizes of the materials were characterized by transmission electron microscopy (TEM, JOEP JEM-2010, JEOL Ltd.) operating at 200 kV, and thermal field emission environmental SEM-EDS-EBSD (Quanta 400F, FEI/OXFORD/HKL, Czech/France). The BET surface area, pore volume and pore diameter were determined on a Physical Adsorption Instrument (ASAP 2400, Micrometeritics Co., USA). The structures were determined on an X-ray diffractometer (XRD, D/Max-IIIA, Rigaku Co., Japan, CuK1, $\lambda = 1.54056$ Å radiation).

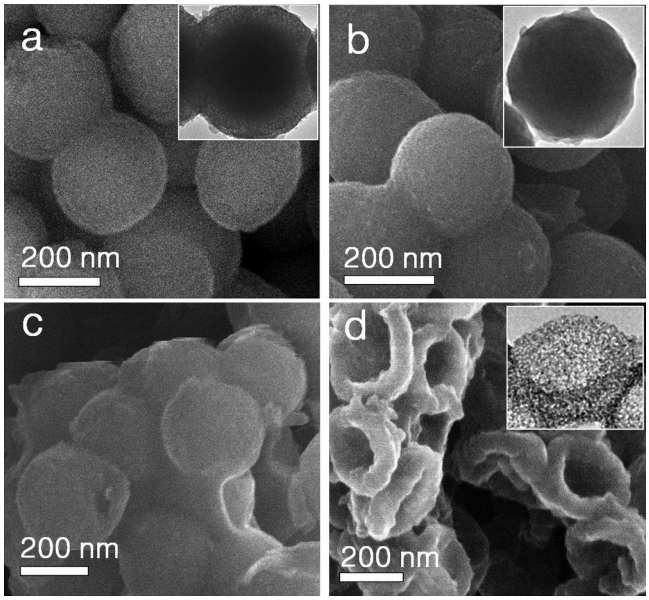

Fig. 2. SEM images of (a) SCMSSs, (b) glucose/SCMSS composite, (c) BLC/SCMSS composite and (d) BLCs; insets in panels a, b and d are the corresponding TEM images.

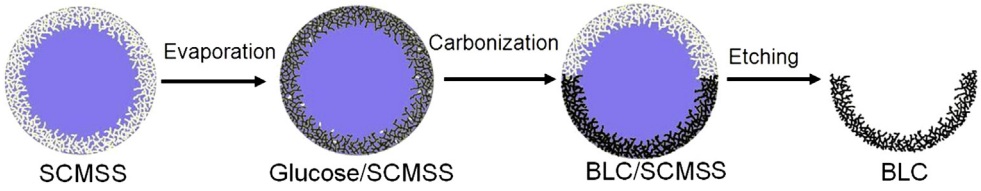

Fig. 1. Schematic synthesis procedure of the BLCs.

Table 1
BET analysis data of the BLCs.

Total surface area ($m^2\ g^{-1}$)	Micropore area ($m^2\ g^{-1}$)	Total pore volume ($cm^3\ g^{-1}$)	Micropore volume ($cm^3\ g^{-1}$)	Average pore diameter (nm)
1108.3	127.2	2.7	0.05	9.4

3. Results and discussion

Fig. 1 illustrates the synthesis procedure of BLCs. The first step is to fill glucose into the mesoporous shell of the SCMSSs to form glucose/SCMSS composite during the evaporation process. The second step is to melt the glucose, and let the melted glucose flow down along the mesopores of the SCMSSs to form BLC/SCMSS composite during carbonization process. The final step is to remove the SCMSSs by HF solution etching to form the final BLCs.

Fig. 2a shows the synthesized SCMSS templates, which are uniform with the diameter of about 300 nm. The inset TEM image in Fig. 2a clearly shows the solid core and mesoporous structure of an SCMSS with the core diameter of 200 nm and shell thickness of 50 nm. Fig. 2b shows the SEM image of the glucose/SCMSS composite, which has the similar diameter as the SCMSSs. The inset TEM image in Fig. 2b proves that the glucose has been successfully filled into mesoporous shell of the SCMSS. Fig. 2c shows the SEM image of the BLC/SCMSS composite, which is obtained after the glucose flowing. The borderline between the SCMSS and the carbonized glucose can be seen. Fig. 2d is the SEM image of the BLCs, showing regular bowl shape, indicating the SCMSS templates having successfully been removed with HF solution etching. The

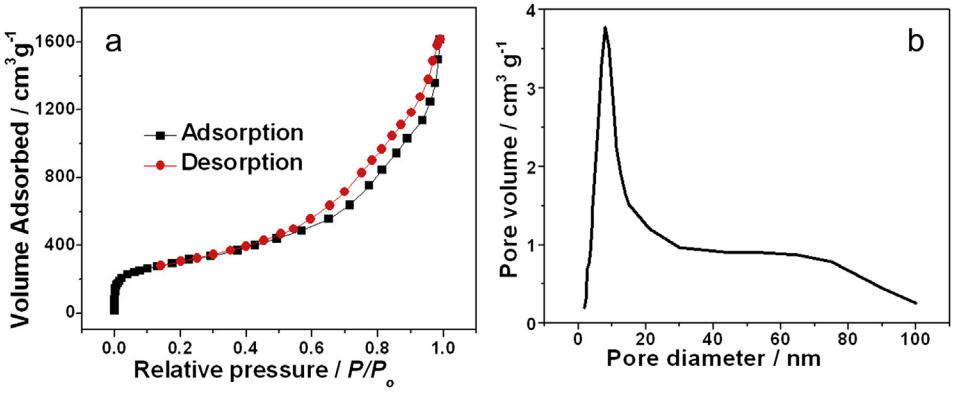

Fig. 3. (a) N_2 adsorption and desorption isotherms, (b) pore size distribution for the BLCs.

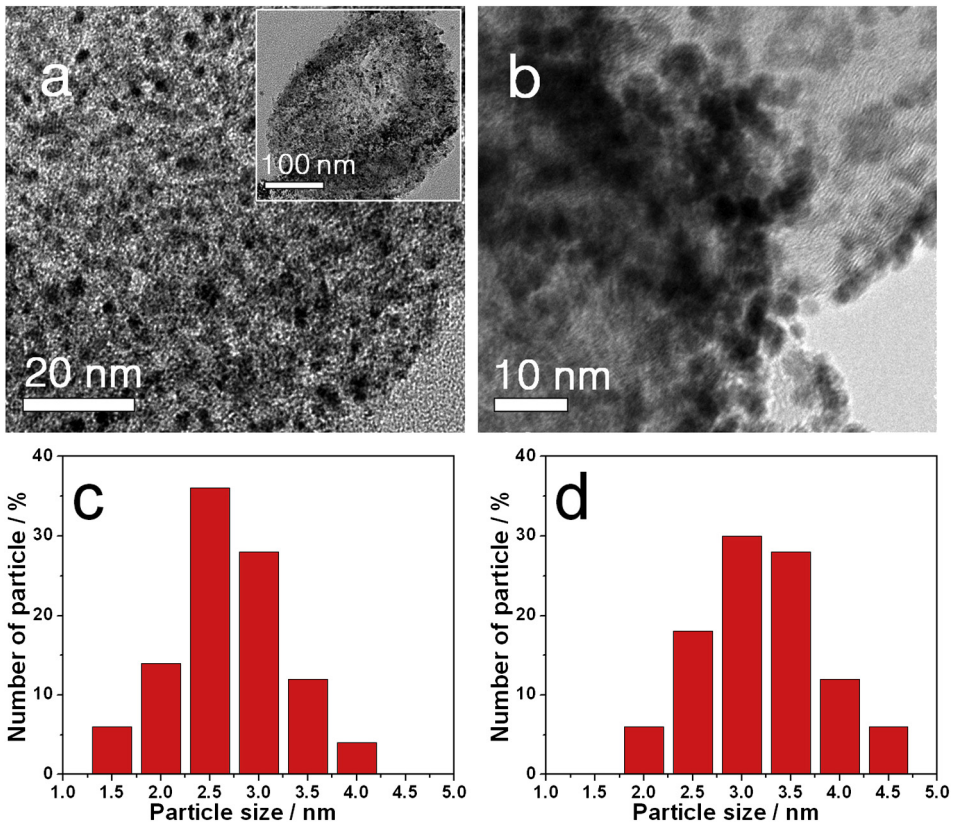

Fig. 4. (a) TEM image of Pt/BLC, inset is the minified TEM image, (b) TEM image of Pd/C (Syns); (c) and (d) are the Pt particle size distributions in Pt/BLC and Pt/C (Syns).

inset TEM image in Fig. 2d clearly proves the mesoporous structure of the BLCs.

The N_2 isotherms (Fig. 3a) and pore size distribution (Fig. 3b) for the BLCs were obtained, and the corresponding BET data were summarized in Table 1. The results exhibit that the BLCs have a specific surface area of 1108.3 $m^2\ g^{-1}$, pore volume of 2.7 $cm^3\ g^{-1}$ and average pore diameter of 9.4 nm, indicating that the pores on BLCs are dominantly mesopores.

The BLCs were used as support to load Pt nanoparticles for methanol oxidation and ORR. Fig. 4a is the TEM image of Pt/BLC, inset is the corresponding minified TEM image. The images show that Pt particles are uniformly dispersed on the surface of BLCs. Fig. 4b is the TEM image of the Pt/C (Syns), which also shows uniform dispersion of Pt particles, however, the Pt particles are too densely collected, which might lead to low use ratio and poor mass transfer. Fig. 4c and d shows Gaussian distributions of Pt particle sizes on both BLCs and Vulcan XC-72 carbon, based respectively on 50 Pt particles randomly selected. The average Pt particle sizes in Pt/BLC and Pt/C (Syns) are calculated as 2.7 and 3.2 nm.

Fig. 5 shows the XRD patterns of the Pt/BLC and Pt/C (Syns). The peaks at 2θ of 39.8°, 46.2° and 67.5° correspond to (111), (200) and (220) facets of Pt crystal respectively. The Pt (220) peak was used to calculate the particle size according to the Scherrer's equation (1).

$$D = K\lambda/(B\cos\theta) \quad (1)$$

where D denotes the average diameter in nm, K the Scherrer constant (0.89), λ the wavelength of X-ray ($\lambda = 0.154056$ nm), B the corresponding full width at half maximum of the (220) diffraction peak and θ the Bragg's diffraction angle. The Pt particle sizes in Pt/BLC and Pt/C (Syns) are calculated as 2.5 and 3.3 nm respectively, which are consistent with the TEM results.

Obviously, the BLC favors the formation of smaller Pt particles, which should be closely related to surface structure of the BLCs. On one hand, the BLCs have much high surface area (1108.3 $m^2\ g^{-1}$), which benefit the dispersion of the loaded Pt particles; on the other hand, it can be imagined that mesopores of BLCs (2.7 $cm^3\ g^{-1}$ in pore volume) could restrict the movement and shedding of the Pt particles due to strong physical interaction force, therefore, favor the stable attachment of smaller Pt particles.

Fig. 6a compares the performances of methanol oxidation on Pt/BLC, Pt/C (Syns) and Pt/C (TKK) electrodes at the same Pt loadings. Table 2 summarizes the peak current densities and Pt mass contents for the three electrocatalysts. The Pt/BLC shows a high peak current density of 1846 mA mg_{Pt}^{-1}, which is 2.6 times that of Pt/C

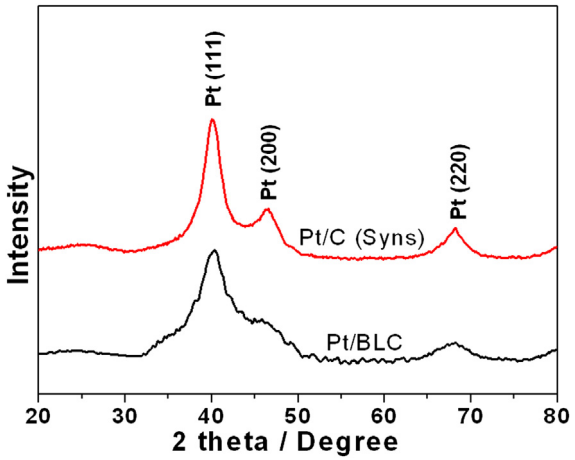

Fig. 5. XRD patterns of Pt/BLC and Pt/C (Syns).

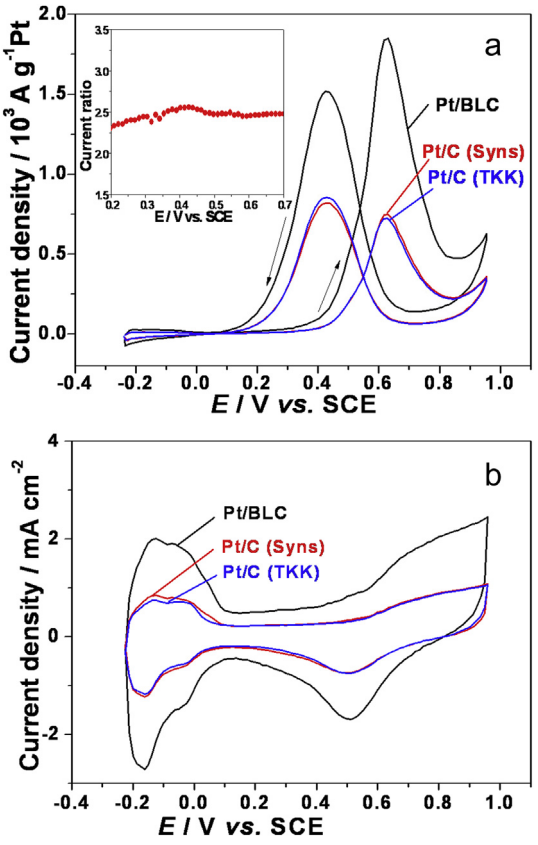

Fig. 6. (a) Cyclic voltammograms of methanol oxidation on Pt/BLC, Pt/C (Syns) and Pt/C (TKK) electrodes in 0.5 mol L^{-1} H_2SO_4/1.0 mol L^{-1} methanol solution at 30 °C, scan rate: 50 mV s^{-1}; inset is the plot of the ratio of the current density on Pt/BLC to the current density on Pt/C (TKK); (b) cyclic voltammograms on the three electrodes in 0.5 mol L^{-1} H_2SO_4 solution at 30 °C, scan rate: 50 mV s^{-1}.

(TKK, 723 mA mg_{Pt}^{-1}). The inset in Fig. 6a shows the plot of the ratio of the current density on Pt/BLC to the current density on Pt/C (TKK). It can be seen that Pt/BLC has slightly more advantage in current density than Pt/C (TKK) around 0.4 V compared to peak current potential. The results prove that the BLCs as support significantly improve the use ratio of the noble metal particles, which were further evidenced by comparing the electrochemical active surface area (EASA). The EASAs for the three electrodes can be calculated from Fig. 6b (assuming that $Q_H = 210\ \mu C\ cm^{-2}$ for a smooth polycrystalline Pt [40]) and the results were listed in Table 2. As can be seen that the EASA ratio of Pt/BLC to Pt/C (TKK) is 3.0, while the peak current density ratio of Pt/BLC to Pt/C (TKK) for methanol oxidation is 2.6. So the current enhancement for methanol oxidation should result from surface area effect. The current density ratio (2.6) being less than the EASA ratio (3.0) is due to the concentration polarization. Furthermore, it is obvious that the mesoporous and bowl structure of the BLCs as support definitely improves the mass transfer for the electrochemical reactions

Table 2
The methanol oxidation performances of the three electrocatalysts.

Electrocatalyst	Pt mass content[a]	EASA/$m^2\ g^{-1}$	Peak current density/mA mg_{Pt}^{-1}
Pt/BLC	48.1%	137.1	1846
Pt/C (Syns)	47.3%	55.4	745
Pt/C (TKK)	47.6%	45.7	723

[a] The data were determined by inductively coupled plasma-atomic emission spectrometry (ICP).

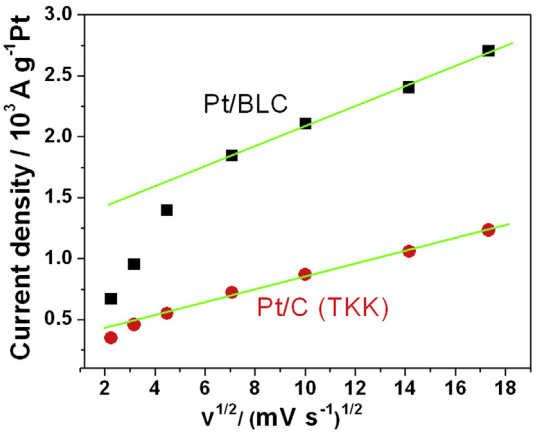

Fig. 7. Plots of the peak current density against the square root of the scan rate for both electrodes.

compared to the carbon powder support. This is extremely important for the direct alcohol fuel cells. In addition, it is noticed that the Pt/C (Syns) synthesized by ourselves has slightly better performances than the commercial Pt/C (TKK) electrocatalyst at the same Pt loadings.

The improved mass transfer property of the Pt/BLC electrocatalyst was evidenced by performing various scan rates for methanol oxidation (Fig. 7). The deflection from the linear line of the data at lower scan rates in the relationship of peak current

Table 3
The ORR mass activities of the three electrocatalysts.

Electrocatalyst	Pt/BLC	Pt/C (Syns)	Pt/C (TKK)
i_m at 0.9 V/mA mg_{Pt}^{-1}	180.6	124.4	116.2

density and square root of scan rate on electrode indicates the improvement in the mass transfer. The straight line appears over the scan rate of 50 mV s^{-1} on Pt/BLC, indicating improved mass transfer; however, it shows a linear line at any scan rate on Pt/C (TKK) electrode, indicating the concentration polarization. It is worthy of being mentioned that early literatures [7–10,41] reported that methanol oxidation currents at the peak potential range were not under complete mass transfer control, methanol concentration, Pt crystal form and pretreatment of Pt surface were all important factors to affect the methanol oxidation current density.

The Pt/BLC was further tested for ORR. Fig. 8a shows the linear polarization curves of ORR on Pt/BLC, Pt/C (Syns) and Pt/C (TKK) electrodes in O_2 saturated 0.1 mol L^{-1} $HClO_4$ solution with a scan rate of 5 mV s^{-1} and rotating speed of 1600 rpm min^{-1} at 25 °C. Fig. 8b shows the kinetic current of the electrocatalysts calculated from the experimental data using the mass transport correction for rotating disk electrode [42]:

$$i_k = i_d i/(i_d - i) \quad (2)$$

where i is the experimentally obtained current, i_d refers to the measured diffusion-limited current and i_k the mass-transport-free

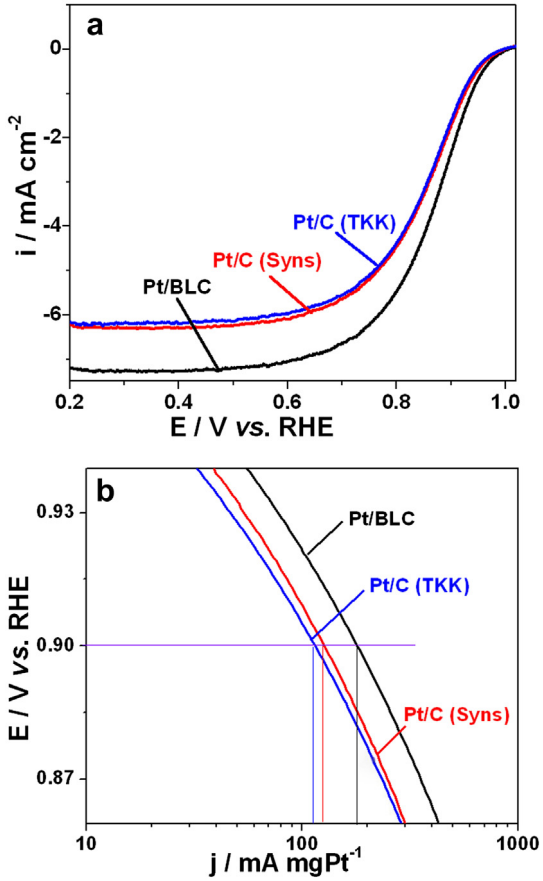

Fig. 8. (a) The ORR on Pt/BLC, Pt/C (Syns) and Pt/C (TKK) electrodes in O_2 saturated 0.1 mol L^{-1} $HClO_4$ solution, 25 °C, scan rate: 5 mV s^{-1}, 1600 rpm; (b) the corresponding mass activity–potential plots.

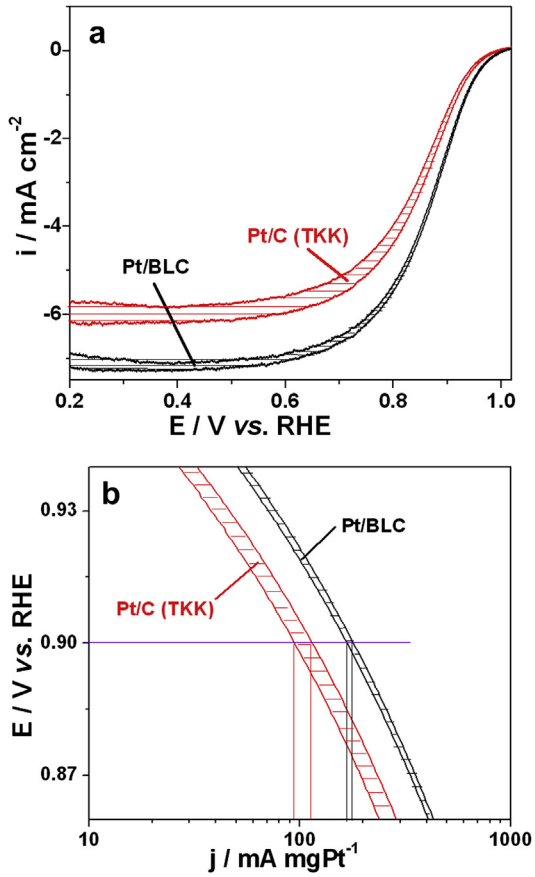

Fig. 9. (a) The ORR on Pt/BLC and Pt/C (TKK) at 1st and 10,000th cyclic voltammogram cycles in O_2 saturated 0.1 mol L^{-1} $HClO_4$ solution with the scan rate of 5 mV s^{-1} at 25 °C, 1600 rpm min^{-1}, (b) the corresponding mass activity–potential plots.

kinetic current. The mass activity (i_m) can be determined via the calculation of i_k using equation (2) and normalized to the Pt loadings. The kinetic currents measured from the curves in Fig. 8b are summarized in Table 3.

Among the three electrocatalysts, Pt/BLC has the highest catalytic activity for ORR and the Pt-mass activity was measured as 180.6 mA mg_{Pt}^{-1}, which is 1.6 times that of the commercial Pt/C (TKK, 114.2 mA mg_{Pt}^{-1}) electrocatalyst. The Pt/C (Syns) and Pt/C (TKK) were not as good as Pt/BLC for ORR due to that they had too dense Pt particles and inferior mass transfer, not fully use all the Pt particles. The results are consistent with the methanol oxidation results (Figs. 6 and 7). Moreover, Fig. 8a shows that the Pt/BLC has higher limiting current density than both Pt/C (Syns) and Pt/C (TKK), confirming the better mass transfer of Pt/BLC. In this study, the measured activities of the Pt/C (Syns) are slightly better than that of Pt/C (TKK) electrocatalyst, and they are all in agreement with the published value in the literature [43].

The stabilities of the Pt/BLC and Pt/C (TKK) for ORR are shown in Fig. 9a. Fig. 9b is the corresponding mass activity–potential plots. The shadows in Fig. 9a and b are the cycling difference between the 1th cycle and the 10,000th cycle. It is clear that the activity of the commercial Pt/C reduced 18.9% from 116.2 mA mg_{Pt}^{-1} to 94.2 mA mg_{Pt}^{-1} by comparing the Pt-mass activity at 0.9 V. However, the activity of the Pt/BLC reduced 6.9% from 180.6 mA mg_{Pt}^{-1} to 168.1 mA mg_{Pt}^{-1} The results indicate that Pt/BLC electrocatalyst is much stable than that of the commercial Pt/C (TKK) electrocatalyst, confirming that mesoporous structure of BLCs favors the stable attachment of the loaded Pt particles.

4. Conclusions

BLCs were prepared using glucose as carbon source and SCMSSs as templates. Compared to carbon powders, the high surface area, bowl and mesoporous structure of the BLCs are beneficial for the uniform dispersion and stable loading of smaller Pt particles, and improve the mass transfer and stability in catalyzing both methanol oxidation and ORR. The current densities on Pt/BLC electrocatalyst were 2.6 times for methanol oxidation and 1.6 times for ORR as high as that of Pt/C (TKK), being promising candidate for fuel cell electrocatalyst.

Acknowledgments

This work was financially supported by China Postdoctoral Science Foundation (2012M521011), College Natural Science Research Program of Jiangsu Province (12KJB150007). Mingmei Zhang thanks the support by Innovation Funds of Jiangsu University (CXLX12_0647). Jimin Xie thanks the Science and Technology Support Program of Jiangsu (BE2010144), Natural Science Foundation of Jiangsu (BK2010166) and Social Development Program of Zhenjiang (SH2010025).

References

[1] M. Yazdanpour, A. Esmaeilifar, S. Rowshanzamir, Int. J. Hydrogen Energy 37 (2012) 11290–11298.
[2] R.L. Borup, J.R. Davey, F.H. Garzon, D.L. Wood, M.A. Inbody, J. Power Sources 163 (2006) 76–81.
[3] M. Wu, P.K. Shen, Z. Wei, S. Song, M. Nie, J. Power Sources 166 (2007) 310–316.
[4] K. Gong, D. Su, R.R. Adzic, J. Am. Chem. Soc. 132 (2010) 14364–14366.
[5] S.Y. Huang, P. Ganesan, B.N. Popov, ACS Catal. 2 (2012) 825–831.
[6] M. Nie, P.K. Shen, M. Wu, Z. Wei, H. Meng, J. Power Sources 162 (2006) 173–176.
[7] D. Pletcher, V. Solis, Electrochim. Acta 27 (1982) 775–782.
[8] J. Clavilier, C. Lamy, J.M. Leger, J. Electroanal. Chem. 125 (1981) 249–254.
[9] C. Lamy, Electrochim. Acta 29 (1984) 1581–1588.
[10] A. Papoutsis, J.-M. Leger, C. Lamy, J. Electroanal. Chem. 234 (1987) 315–327.
[11] R.H. Wang, Y. Xie, K.Y. Shi, J.Q. Wang, C.G. Tian, P.K. Shen, H. Fu, Chem.—Eur. J. 18 (2012) 7443–7451.
[12] B. Fang, J.H. Kim, J.S. Yu, Electrochem. Commun. 10 (2008) 659–662.
[13] J.D. Qiu, G.C. Wang, R.P. Liang, X.H. Xia, H.W. Yu, J. Phys. Chem. C 115 (2011) 15639–15645.
[14] F. Su, Z. Tian, C.K. Poh, Z. Wang, S.H. Lim, Z. Liu, J. Liu, Chem. Mater. 22 (2010) 832–839.
[15] M. Zhang, Z. Yan, Q. Sun, J. Xie, J. Jing, New J. Chem. 36 (2012) 2533–2540.
[16] J. Liu, Z. Li, C. He, R. Fu, D. Wu, S. Song, Int. J. Hydrogen Energy 36 (2011) 2250–2257.
[17] S. Sharma, B.G. Pollet, J. Power Sources 208 (2012) 96–119.
[18] J. Solla-Gullón, F.J. Vidal-Iglesias, J.M. Feliu, Annu. Rep. Prog. Chem., Sect. C: Phys. Chem. 107 (2011) 263–297.
[19] J.Y. Choi, R.S. Hsu, Z. Chen, J. Phys. Chem. C 114 (2010) 8048–8053.
[20] Z. Wu, Y. Lv, Y. Xia, P.A. Webley, D. Zhao, J. Am. Chem. Soc. 134 (2012) 2236–2245.
[21] S. Zhang, Y. Shao, G. Yin, Y. Lin, J. Mater. Chem. A 1 (2013) 4631–4641.
[22] Y.Y.J. Tong, Chem. Soc. Rev. 41 (2012) 8195–8209.
[23] T. Fujigaya, M. Okamoto, N. Nakashima, Carbon 47 (2009) 3227–3232.
[24] Z.Z. Zhao, X. Fang, Y.L. Li, Y. Wang, P.K. Shen, F.Y. Xie, X. Zhang, Electrochem. Commun. 11 (2008) 290–293.
[25] X. Wang, C. Hu, Y. Xiong, H. Liu, G. Du, X. He, J. Power Sources 196 (2011) 1904–1908.
[26] Z. Yan, G. He, G. Zhang, H. Meng, P.K. Shen, Int. J. Hydrogen Energy 35 (2010) 3263–3269.
[27] Y.H. Qin, H.H. Yang, X.S. Zhang, P. Li, X.G. Zhou, L. Niu, W.K. Yuan, Carbon 48 (2010) 3323–3329.
[28] C. Huang, C. Li, G. Shi, Energy Environ. Sci. 5 (2012) 8848–8868.
[29] J. Zang, Y. Wang, L. Bian, J. Zhang, F. Meng, Y. Zhao, R. Lu, X. Qu, S. Ren, Carbon 50 (2012) 3032–3038.
[30] F.P. Hu, Z. Wang, Y. Li, C. Li, X. Zhang, P.K. Shen, J. Power Sources 177 (2008) 61–66.
[31] J.H. Bang, Electrochim. Acta 56 (2011) 8674–8679.
[32] J.B. Joo, P.K. Kim, W. Kim, J. Kim, J. Yi, Catal. Today 111 (2006) 171–175.
[33] P.V. Shanahan, L. Xu, C. Liang, M. Waje, S. Dai, Y.S. Yan, J. Power Sources 185 (2008) 423–427.
[34] J.H. Nam, Y.Y. Jang, Y.U. Kwon, J.D. Nam, Electrochem. Commun. 6 (2004) 737–741.
[35] G.S. Chai, S.B. Yoon, J.S. Yu, J.H. Chai, Y.E. Sung, J. Phys. Chem. B 108 (2004) 7074–7079.
[36] H. Chang, S.H. Joo, C. Pak, J. Mater. Chem. 17 (2007) 3078–3088.
[37] S.H. Liu, J.R. Wu, Int. J. Hydrogen Energy 37 (2012) 16994–17001.
[38] S. Song, S. Yin, Z. Li, P.K. Shen, R. Fu, D. Wu, J. Power Sources 195 (2010) 1946–1949.
[39] G. Büchel, M. Grün, K.K. Unger, Supramol. Sci. 5 (1998) 253–259.
[40] H.J. Kim, D.Y. Kim, H. Han, Y.G. Shul, J. Power Sources 159 (2006) 484–490.
[41] O.A. Khazova, Y.B. Vasil'ev, V.S. Bagotskii, Bull. Russ. Acad. Sci., Div. Chem. Sci. 14 (1965) 1743–1751.
[42] S. Chouzier, P. Afanasiev, M. Vrinat, T. Cseri, M. Roy-Auberger, J. Solid State Chem. 179 (2006) 3314–3323.
[43] B. Lim, M.J. Jiang, P.H.C. Camargo, E.C. Cho, J. Tao, X.M. Lu, Y.M. Zhu, Y.A. Xia, Science 324 (2009) 1302–1305.